Workshop on Fission Dynamics 2026

Why do the fission fragments spin

Guillaume SCAMPS

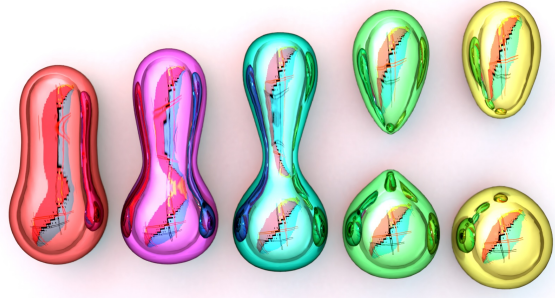

Université de Toulouse

L2IT

cnrs

TDHFB equations

$$i\hbar\frac{\partial}{\partial t}\begin{pmatrix} U \\ V \end{pmatrix} = \begin{pmatrix} h(t) & \Delta(t) \\ -\Delta^*(t) & -h^*(t) \end{pmatrix}\begin{pmatrix} U \\ V \end{pmatrix}$$

TDHFB equations

$$i\hbar\frac{\partial}{\partial t}\begin{pmatrix} U \\ V \end{pmatrix} = \begin{pmatrix} h(t) & \Delta(t) \\ -\Delta^*(t) & -h^*(t) \end{pmatrix}\begin{pmatrix} U \\ V \end{pmatrix}$$

Strengths

- Self-consistent mean field + pairing
- Functional and no other adjustable parameters.
- One-body dissipation
- Large-amplitude collective motion

TDHFB equations

$$i\hbar\frac{\partial}{\partial t}\begin{pmatrix} U \\ V \end{pmatrix} = \begin{pmatrix} h(t) & \Delta(t) \\ -\Delta^*(t) & -h^*(t) \end{pmatrix}\begin{pmatrix} U \\ V \end{pmatrix}$$

Strengths

- Self-consistent mean field + pairing
- Functional and no other adjustable parameters.
- One-body dissipation
- Large-amplitude collective motion

Limitations

- Missing quantum and statistic fluctuations
- Broken symmetries (projection needed)
- Computationally expensive

TDHFB equations

$$i\hbar\frac{\partial}{\partial t}\begin{pmatrix} U \\ V \end{pmatrix} = \begin{pmatrix} h(t) & \Delta(t) \\ -\Delta^*(t) & -h^*(t) \end{pmatrix}\begin{pmatrix} U \\ V \end{pmatrix}$$

TDBCS approximation

Canonical basis evolution :

$$i\hbar\,\dot{\varphi}_\alpha = h\,\varphi_\alpha$$

$$i\hbar\,\dot{n}_\alpha = \kappa_\alpha\Delta_\alpha^* - \kappa_\alpha^*\Delta_\alpha$$

$$i\hbar\,\dot{\kappa}_\alpha = 2\epsilon_\alpha\kappa_\alpha + \Delta_\alpha(2n_\alpha - 1)$$

Strengths

- Self-consistent mean field + pairing
- Functional and no other adjustable parameters.
- One-body dissipation
- Large-amplitude collective motion

Limitations

- Missing quantum and statistic fluctuations
- Broken symmetries (projection needed)
- Computationally expensive

Spin of the fragments

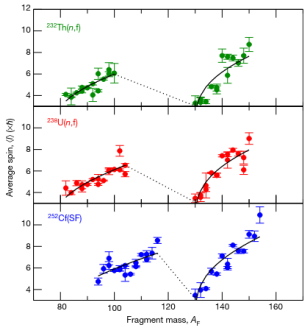

Correlations

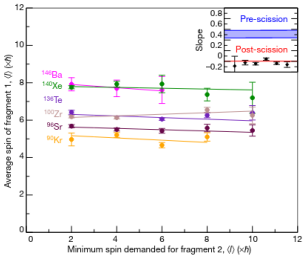

J. N. Wilson, Nature, 590, 566 (2021)

- The average spin follows a sawtooth shape
- No correlations between the spins of the fragments

Spins are mostly perpendicular to the fission axis

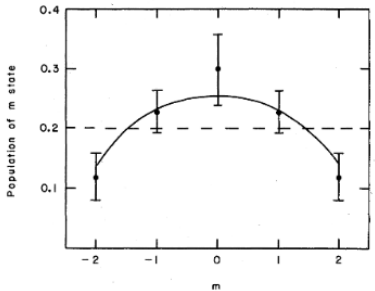

FIG. 9. The points are the calculated populations of the various m substates of the 2^+ level in ^{144}Ba. These values were determined using the fitted experimental angular distribution of the $2^+ \rightarrow 0^+$ γ ray. The solid line represents the predicted population of the m states as calculated from the statistical-model analysis of the de-excitation process using Eqs. (4) and (5) with an assumed value of $B=6$ [Eq. (3)] for the initial angular momentum distribution.

J. B. Wilhelmy, E. Cheifetz, R. C. Jared, S. G. Thompson, H. R. Bowman, and J. O. Rasmussen Phys. Rev. C 5, 2041 (1972)

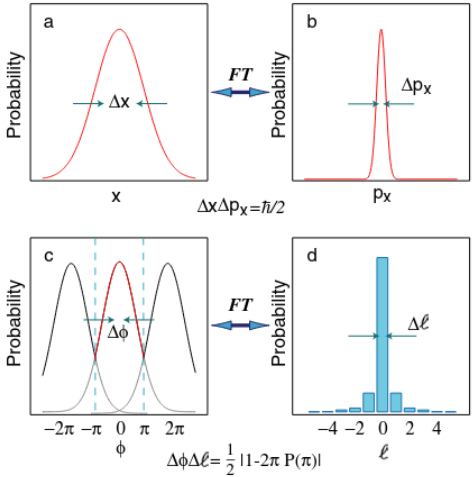

S. Franke-Arnold, et al. New Journal of Physics 6, 103 (2004)

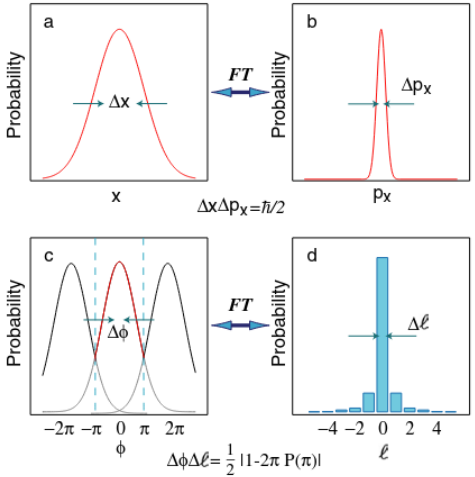

S. Franke-Arnold, et al. New Journal of Physics 6, 103 (2004)

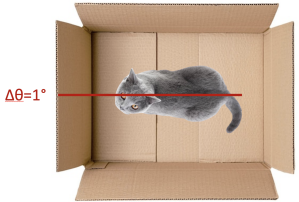

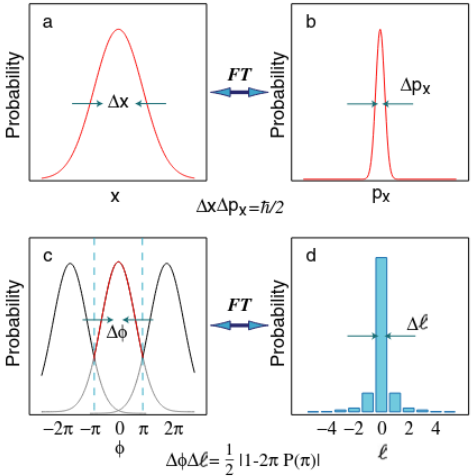

S. Franke-Arnold, et al. New Journal of Physics 6, 103 (2004)

For $\Delta\Theta = 1°$, $\Delta L = 29\hbar$.
For a cat, angular velocity $\omega = 10^{-33}s^{-1}$

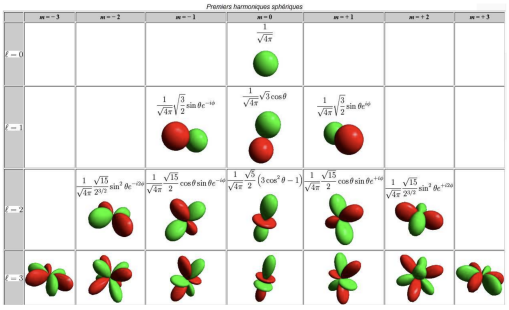

Orientation pumping mechanism

Isotropic potential at scission

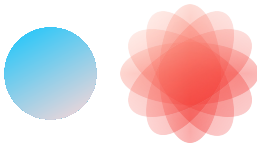

Confining potential at scission

L. Bonneau, P. Quentin, and I. N. Mikhailov, PRC 75, 064313 (2007).

For $\Delta\Theta = 1^\circ$, $\Delta L = 29\hbar$.

For a nucleus, angular velocity $\omega = 10^{20} s^{-1}$

^{144}Ba + ^{96}Sr at 16 Fm, Θ_{ini}=25 deg, Functional : Skyrme Sly4d

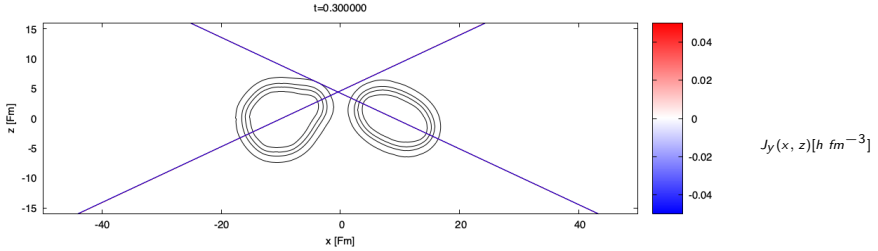

G. Scamps, PRC 106, 054614 (2022).

One body-evolution - One body-observable

^{144}Ba + ^{96}Sr at 16 Fm, Θ_{ini}=25 deg, Functional : Skyrme Sly4d

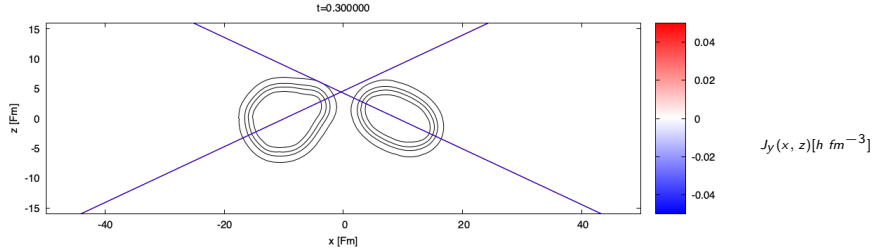

G. Scamps, PRC 106, 054614 (2022).

One body-evolution - One body-observable

^{144}Ba + ^{96}Sr at 16 Fm, Θ_{ini}=25 deg, Functional : Skyrme Sly4d

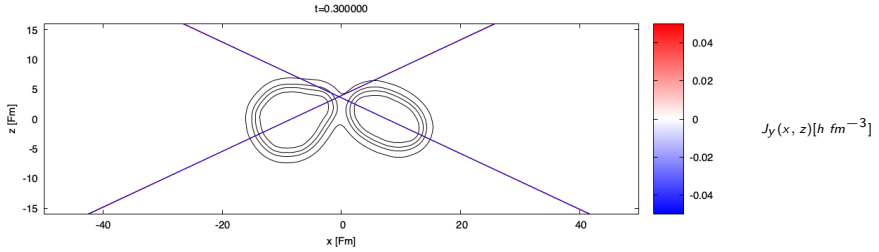

G. Scamps, PRC 106, 054614 (2022).

^{144}Ba + ^{96}Sr at 16 Fm, Θ_{ini}=25 deg, Functional : Skyrme Sly4d

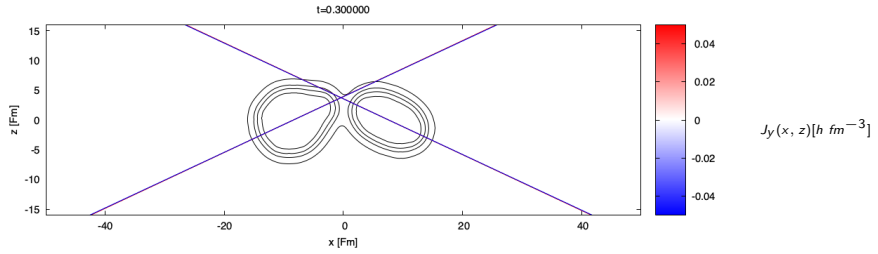

G. Scamps, PRC 106, 054614 (2022).

Nucleus-nucleus potential at scission

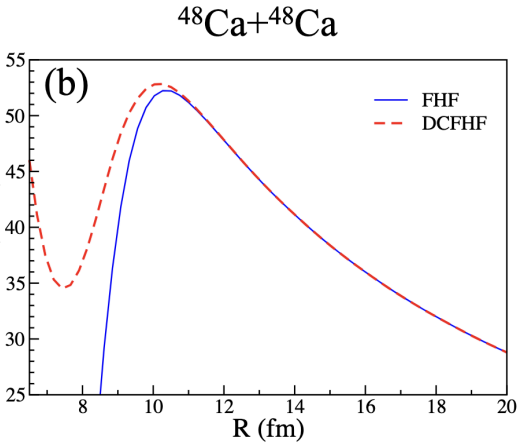

C. Simenel, A. S. Umar, K. Godbey, M. Dasgupta, and D. J. Hinde, Phys. Rev. C 95, 031601 (2017)

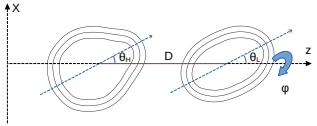

Potential as a function of the light fragment angle

$^{132}Sn+^{108}Ru$

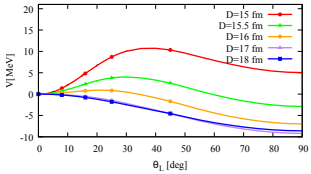

Two torques :

- attractive nucleus-nucleus torque
- repulsive Coulomb torque

Potential as a function of the light fragment angle

$^{144}Ba+^{96}Sr$. D=15.5 and 20 fm

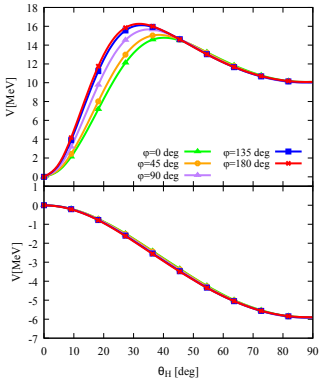

The azimuthal angle doesn't have an important role.

Frozen Hartree-Fock potential

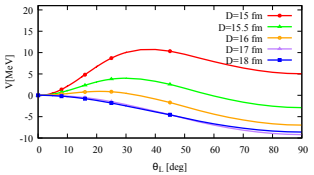

Two torques :

- attractive nucleus-nucleus torque
- repulsive Coulomb torque

4 degrees of freedom

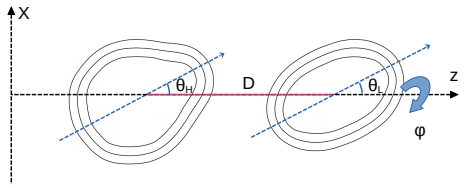

Hamiltonian

$$\hat{H}(D) = \frac{\hbar^2}{2I_H}\hat{L}_H^2 + \frac{\hbar^2}{2I_L}\hat{L}_L^2 + \frac{\hbar^2}{2I_\Lambda(D)}\hat{\Lambda}^2 + \hat{V}(\hat{\Theta}_H, \hat{\Theta}_L, \hat{\varphi}, D)$$

Solved in basis $|L_H, m, L_L, -m\rangle$ **Important :** assume cold rigid fragments

G. Scamps, G. Bertsch, Phys. Rev. C 108, 034616(2023).
Similar to the orientation pumping mechanism model Mikhailov, I. N., and Quentin, P. Physics Letters B, 462(1-2), 7-13 (1999) and Azam Rahmatinejad model

Evolution of a one-angle wave packet assuming spherical ^{132}Sn

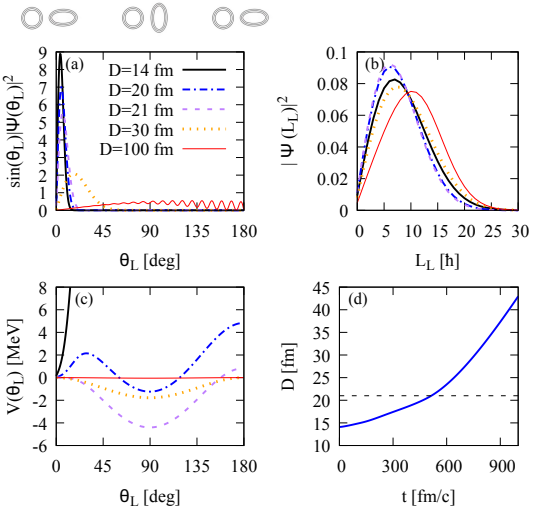

G. Scamps, G. Bertsch, Phys. Rev. C 108, 034616 (2023).

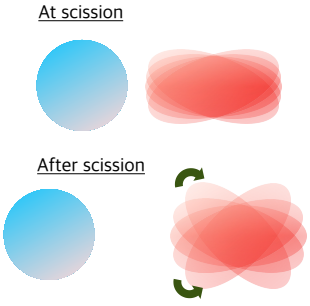

Effect of quadrupole deformation >> effect of $Z_1 Z_2$

TABLE II. Average spin $\langle L^2 \rangle^{\frac{1}{2}}$ in unit of $\hbar$ for the three fission fragments at scission ($D = 21$ fm) and at large distances. The last two columns show the same quantity with an MOI divided by 2.

Nucleus	Scission	Final	Scission ($I_{\frac{1}{2}}$)	Final ($I_{\frac{1}{2}}$)
^{108}Ru	9.28	12.31	7.24	10.38
^{144}Ba	10.04	10.95	7.70	8.66
^{96}Sr	7.74	9.30	6.03	7.62

also J. Randrup, PRC 108, 064606 (2023) : increase of 1 to 3 $\hbar$ due to the Coulomb torque.

Correlation between the angular momentum

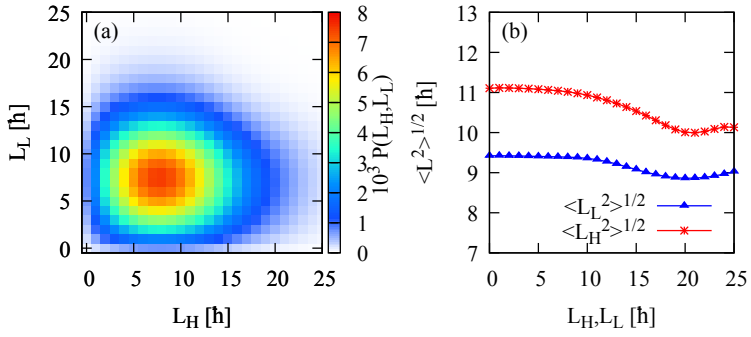

^{144}Ba+^{96}Sr

- No or small correlation observed in the magnitude of the angular momentum.
- More angular momentum for the heavy fragment

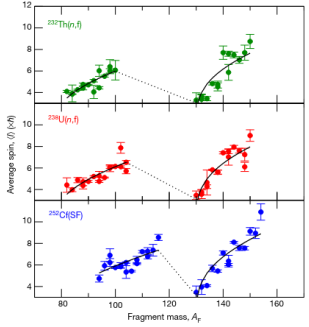

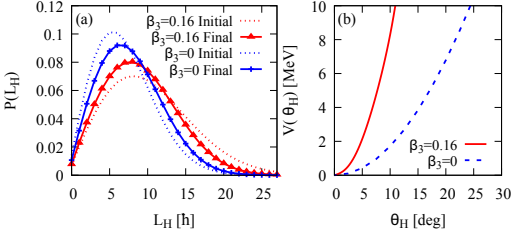

Mechanism

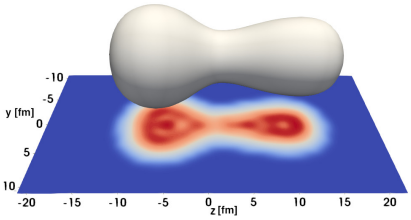

- Pear-shaped deformation plays an important role at scission. G. Scamps C. Simenel, Nature 564, pages 382–385 (2018)
- Octupole deformation makes the angular potential stiffer which increase the zero-point motion → more angular momentum

Orbital angular momemtum

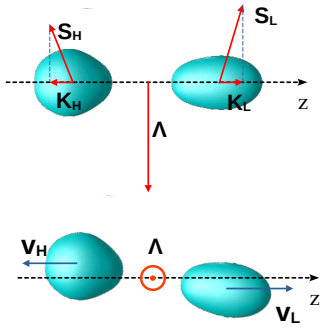

In spontaneous fission of a 0^+ state

$$\mathbf{S_H} + \mathbf{S_L} + \mathbf{\Lambda} = \mathbf{0},$$

Triangular rule :

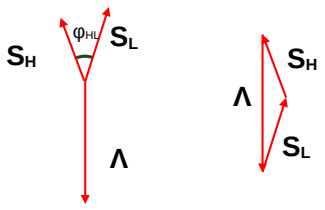

$$\cos(\varphi_{HL}) = \left(\frac{\Lambda(\Lambda+1) - S_H(S_H+1) - S_L(S_L+1)}{2\sqrt{S_H(S_H+1)S_L(S_L+1)}} \right)$$

TDDFT (in 2022) vs Freya

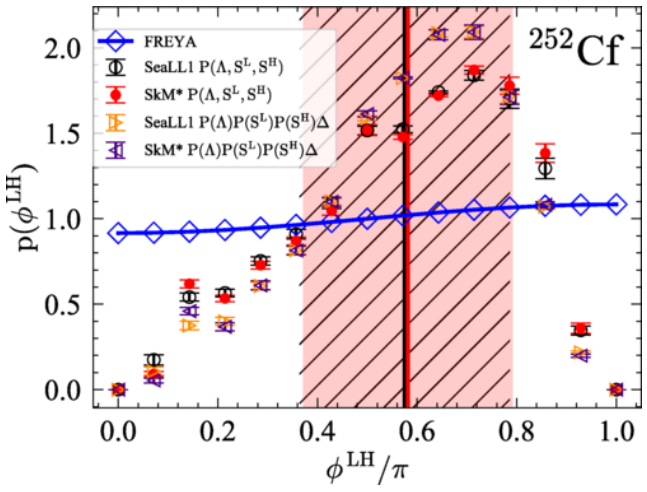

A. Bulgac, I. Abdurrahman, K. Godbey, and I. Stetcu, Phys. Rev. Lett. 128, 022501(2022).

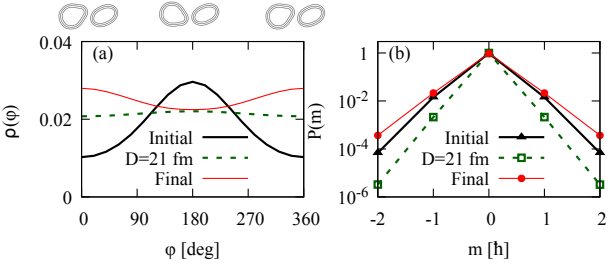

G. Scamps, G. Bertsch, Phys. Rev. C 108, 034616 (2023).

Geometry

- Small azimuthal correlation
- Spins are perpendicular to the fission axis
- Complex pattern in the opening angle, different from previous model

Method

- Quantal collective model → beyond one-body
- Time-dependent evolution of a wave-packet
- Microscopic potential with FHF

Results

- No strong correlation of the magnitude and direction of the spins
- Both spins are oriented in the plane perpendicular to the fission axis.
- The Coulomb interaction induces an increase of the angular momentum by 1 to 3 $\hbar$
- The octupole deformation increases the angular momentum generated at scission

Limitation

- Frozen approximation
- Initial conditions

G. Scamps, G. Bertsch, Phys. Rev. C 108, 034616 (2023).

Projection method

Projection on the spin and K number (Projection of the spin on the fission axis)

$$\hat{P}^{S}_{MK} = \frac{(2S+1)}{16\pi^2} \int d\Omega \mathcal{D}^{S*}_{MK}(\Omega)\, e^{i\alpha \hat{S}_z} e^{i\beta \hat{S}_y} e^{i\gamma \hat{S}_z},$$

$$P(S_F, K_F) = \langle \Psi | \hat{P}^{S_F}_{K_F K_F} | \Psi \rangle,$$

Calculation of the overlap : G. F. Bertsch and L. M. Robledo, PRL 108, 042505 (2012)

$$\langle \Psi | \hat{R} | \Psi \rangle = \frac{(-1)^n}{\prod_\alpha^n v_\alpha^2} \mathrm{pf} \begin{bmatrix} V^T U & V^T R^T V^* \\ -V^\dagger R V & U^\dagger V^* \end{bmatrix}$$

Optimized Pfaffian calculation : M. Wimmer, ACM Trans. Math Softw. 38, 30 (2012).

Spin distribution in the fragments

Obtained using 3-angle projection operator

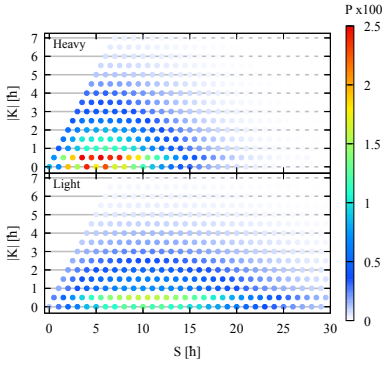

Geometry of the reaction

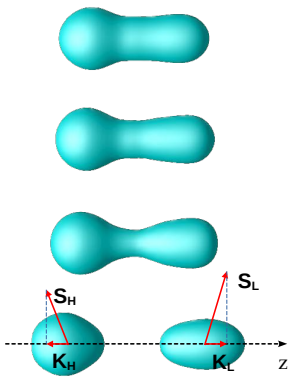

G.scamps, I. Abdurrahman, M. Kafker, A. Bulgac, and I. Stetcu, PRC 108 (6), L061602

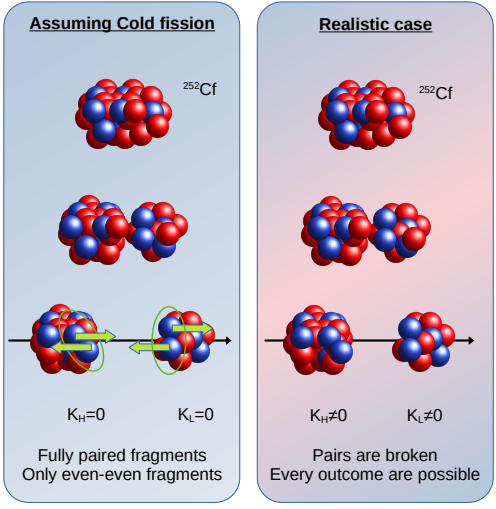

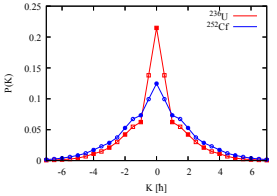

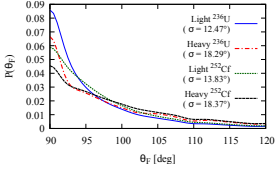

$$\cos\theta_F = \frac{K_F}{\sqrt{S_F(S_F+1)}}$$

G.scamps, I. Abdurrahman, M. Kafker, A. Bulgac, and I. Stetcu, PRC 108 (6), L061602.

$$\varphi_{HL} = \arccos\left(\frac{\Lambda(\Lambda+1) - S_H(S_H+1) - S_L(S_L+1)}{2\sqrt{S_H(S_H+1)S_L(S_L+1)}}\right)$$

$$P(\Lambda, S_H, S_L) = \sum_{k_H k_L} \langle\Psi|\hat{P}^{\Lambda}_{0,0}\hat{P}^{S_H}_{K_H K_H}\hat{P}^{S_L}_{K'_L K_L}|\Psi\rangle.$$

$$P(\Lambda, S_H, S_L) = \sum_{K_H K_L K'_H K'_L} (-1)^{K'_H - K_H + K'_L - K_L}$$

$$C^{\Lambda,0}_{S_H,-K_H,S_L,-K_L} C^{\Lambda,0}_{S_H,-K'_H,S_L,-K'_L} \langle\Psi|\hat{P}^{S_H}_{K_H K'_H}\hat{P}^{S_L}_{K_L K'_L}|\Psi\rangle$$

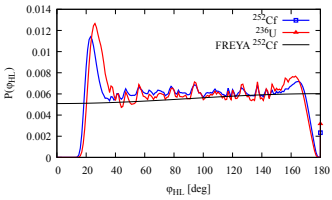

G.scamps, I. Abdurrahman, M. Kafker, A. Bulgac, and I. Stetcu, PRC 108 (6), L061602.

One angle projector :

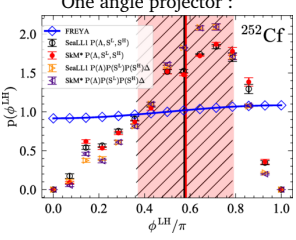

Non alignement of the spins

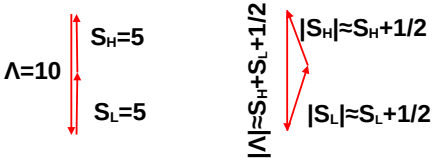

To get a 5 degrees angle between two spins require spins of 262 $\hbar$ and 6565 $\hbar$ for 1 degree

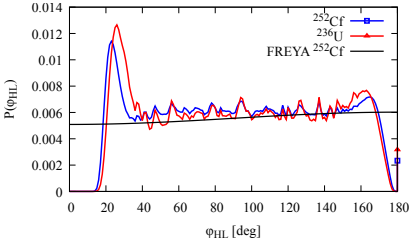

Uncertainty principle in TDDFT

TDHFB framework

- Gogny-TDHFB code
- Gogny D1S interaction
- Hybrid basis :
  - 2D harmonic oscillator (x, y)
  - 1D spatial mesh (z)

Fissioning nuclei

- ^{230}Th
- ^{240}Pu
- ^{250}Cf

Asymmetric fission region
Heavy fragment influenced by octupole deformation

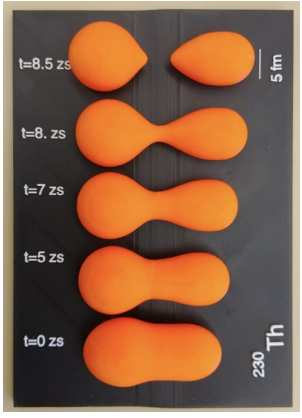

Y. Hashimoto, Time-dependent hartree-fock-bogoliubov calculations using a lagrange mesh with the gogny interaction, PRC 88, 034307 (2013).

Conceptual difficulty

- Unlike position, angular variables are **periodic**.
- Mean values and fluctuations of an angle are not uniquely defined.
- Restrict to well-oriented wave packet

Orientation–angular momentum uncertainty

$$\Delta\theta\,\Delta L_x > \frac{1}{2}, \qquad (L_x \text{ in units of } \hbar)$$

Analogous relation for L_y.

Gaussian orientation state and spin distribution

Gaussian wave packet :

$$\Psi(\theta,\varphi) = \mathcal{N}\exp\left[-\frac{\theta^2}{4\sigma_\theta^2}\right]$$

Spin cut-off distribution :

$$P(L) = \frac{2L+1}{\mathcal{Z}}\exp\left[-\frac{L(L+1)}{2\sigma_L^2}\right]$$

Heisenberg-type relation :

$$\sigma_\theta\,\sigma_L = \frac{1}{2}$$

Second difficulty : composite nuclei

- In collective Hamiltonian models, angle wave packets are well defined.
- In microscopic approaches, orientation is **not an operator**.
- No direct definition of angular fluctuations.

Proposed approach

- Go beyond the one-body density picture.
- Sample nucleon positions and intrinsic spins from the Bogoliubov vacuum.
- Markov Chain Monte Carlo sampling (`NucleoScope`).
- Determine principal axis event-by-event.

Principal axis determination

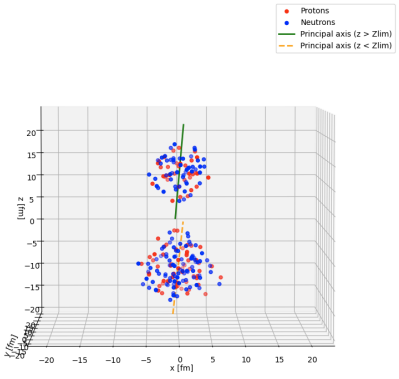

Examples for ^{230}Th.
Red/blue dots : proton/neutron distributions.
Lines : fragment principal axes.

Nucleoscope paper : A. Bernard *et al.*, arXiv :2601.18488 [nucl-th] (2026)

Second difficulty : composite nuclei

- In collective Hamiltonian models, angle wave packets are well defined.
- In microscopic approaches, orientation is **not an operator**.
- No direct definition of angular fluctuations.

Proposed approach

- Go beyond the one-body density picture.
- Sample nucleon positions and intrinsic spins from the Bogoliubov vacuum.
- Markov Chain Monte Carlo sampling (`NucleoScope`).
- Determine principal axis event-by-event.

Principal axis determination

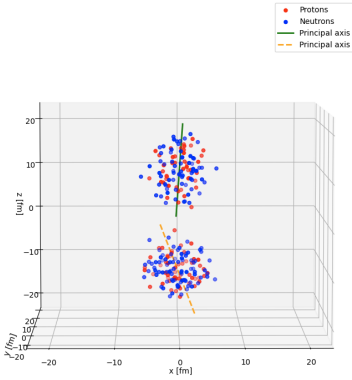

Examples for ^{230}Th.
Red/blue dots : proton/neutron distributions.
Lines : fragment principal axes.

Nucleoscope paper : A. Bernard *et al.*, arXiv :2601.18488 [nucl-th] (2026)

Distribution of θ

- For each sampled event, principal axis of each fragment is computed.
- Obtain θ = angle between fragment axis and global z-axis.
- Construct full probability distribution $P(\theta)$.
- Expectation value $\langle\theta\rangle = 0$ due to symmetry.
- Standard deviation σ_θ characterizes the angular fluctuation.

Physical meaning

- Reflects uncertainty in fragment orientation.
- Geometric definition mainly sensitive to quadrupole deformation.
- Can be used for spin-cutoff estimations.

Angular distribution figure

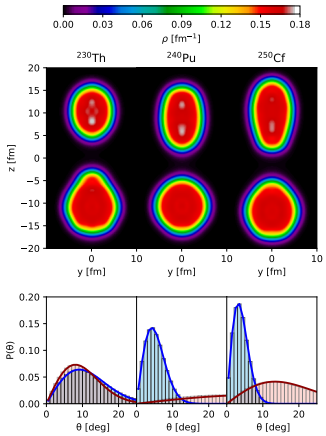

Angular distribution $P(\theta)$ for light (blue) and heavy (red) fragments. Fitted curves illustrate approximate Gaussian behavior.

Nucleoscope paper : A. Bernard *et al.*, arXiv :2601.18488 [nucl-th] (2026)

Angular distribution

$$f(\theta) = \mathcal{N}^2 \sin(\theta) \exp\left[-\frac{\theta^2}{2\sigma_\theta^2}\right]$$

- Excellent agreement with Gaussian form
- Angular fluctuations are Gaussian
- Larger quadrupole deformation $\Rightarrow$ narrower distribution

From σ_θ to spin

$$\sigma_\theta \, \sigma_L = \frac{1}{2}$$

- Extract σ_θ
- Deduce spin cut-off σ_L
- Build spin distribution

Spin distribution

$$P(L) = \frac{2L+1}{\mathcal{Z}} \exp\left[-\frac{L(L+1)}{2\sigma_L^2}\right]$$

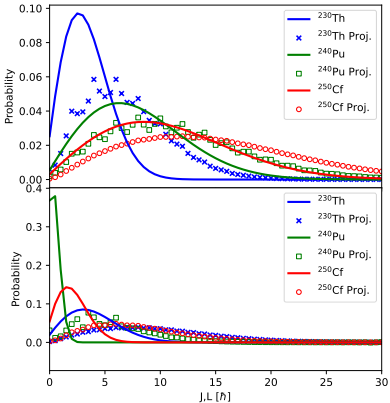

Projection results vs. spin cut-off formula (light : top, heavy : bottom).

Microscopic vs geometric picture

- Exact angular momentum obtained from projection of many-body states.
- Monte Carlo sampling determine the fluctuations of the fragment principal axis from Q_2 deformation.

Octupole deformation

- Principal axis distribution becomes flat.
- Geometric picture underestimates spin.

Spin-cutoff vs deformation

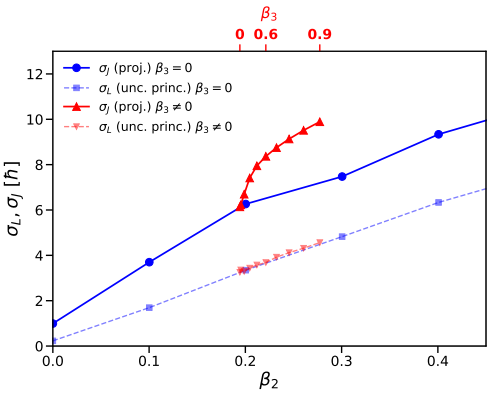

Spin cut-off parameter for ^{144}Ba. Solid lines : projection. Dashed lines : principal-axis uncertainty estimate.

Prolate deformation

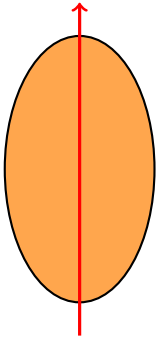

$Q_2 > 0$

Principal axis well defined

Triangular (octupole) configuration

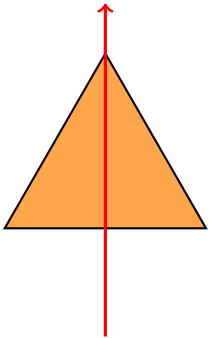

$Q_2 = 0$

Orientation still defined but principal axis isotropic

Overlap of rotated many-body states

$$\langle \Psi | e^{i\alpha \hat{J}_z} e^{i\theta \hat{J}_y} e^{i\gamma \hat{J}_z} | \Psi \rangle \simeq \exp\left[-\frac{\theta^2}{8\sigma_\theta^2} \right]$$

- Gaussian approximation for small rotations
- Width σ_θ characterizes angular localization

Physical meaning

- Many-body state localized in rotational space
- Does **not** rely on geometric definition of orientation
- Orientation angle and angular momentum are conjugate variables

Spin fluctuations

Spin cut-off distribution :

$$P(J) = \frac{2J+1}{\mathcal{Z}} \exp\left[-\frac{J(J+1)}{2\sigma_J^2} \right]$$

$$\sigma_\theta \, \sigma_J = \frac{1}{2}$$

Nucleus	Frag.	σ_L (uncert. with principal axis)	σ_J (overlap)	σ_J (projection)
^{230}Th	L	2.90	5.74	5.81
	H	3.37	7.84	7.88
^{240}Pu	L	6.79	9.32	9.37
	H	0.75	4.67	4.93
^{250}Cf	L	9.00	12.18	12.27
	H	2.12	6.50	6.63

Key result

- Spin cut-off parameters extracted from :
  - angular fluctuations + uncertainty relation
  - Gaussian overlap fit
  - exact angular-momentum projection
- **very good agreement** between overlap and exact projection.
- Error with the principal axis method (miss higher order deformation).

G. Scamps, A. Guilleux, D. Regnier, A. Bernard, Uncertainty Principle and Angular Momentum Generation in Microscopic Fission Models, arXiv :2512.02207 [nucl-th].

Main points

- Orientation-pumping (uncertainty principle) mechanism at scission in collective hamiltonian and TDDFT
- Additional effect of the Coulomb torque
- Internal excitation (breaking of pairs)
- Spins are mainly perpendicular to the fission axis
- Uncorrelated magnitude and orientation of the spins
- Dependence of the mechanism with the deformation (quadrupole and octupole)

Thank you for your attention

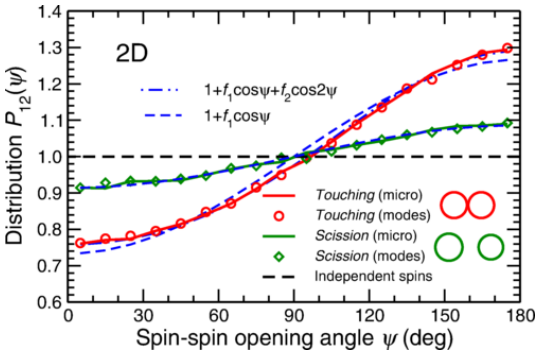

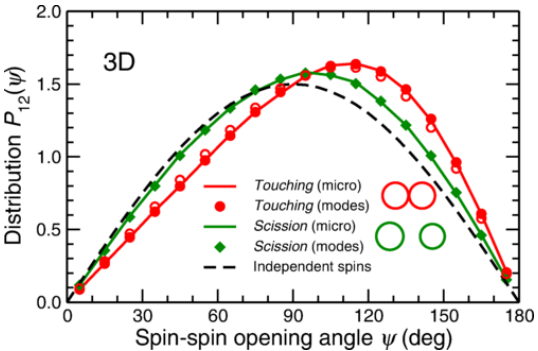

J. Randrup, Phys. Rev. C 106, L051601 (2022).

Question

- How the quantal effects change this picture ?
- How the geometry change the opening angle distribution assuming no correlation ?

Non alignement of the spins

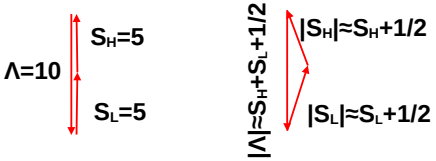

To get a 5 degrees angle between two spins require spins of 262 $\hbar$ and 6565 $\hbar$ for 1 degree

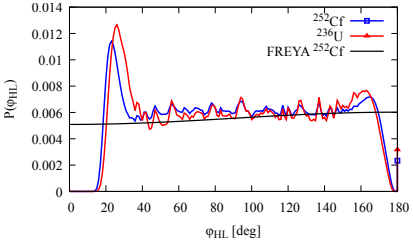

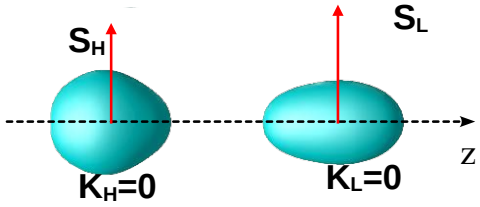

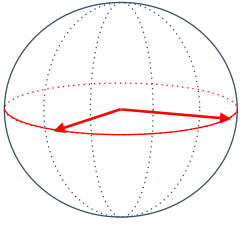

$$|\Psi\rangle = \sum_{s_H,K_H,s_L,K_L} c_{s_H,K_H,s_L,K_L} |s_H, K_H, s_L, K_L\rangle,$$

$$|c_{s_H,K_H,s_L,K_L}|^2 \propto \delta_{K_H,0}\delta_{K_L,0}(2s_H+1)e^{\frac{-s_H(s_H+1)}{2\sigma_H^2}} \times (2s_L+1)e^{\frac{-s_L(s_L+1)}{2\sigma_L^2}}.$$

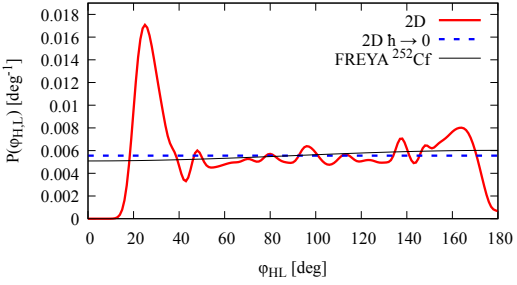

G. Scamps, PRC 109, L011602 (2024).

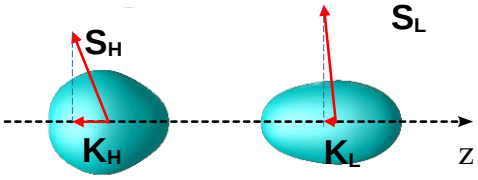

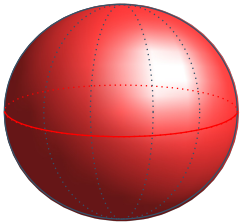

$$|\Psi\rangle = \sum_{S_H,K_H,S_L,K_L} c_{S_H,K_H,S_L,K_L} |S_H, K_H, S_L, K_L\rangle,$$

$$|c_{S_H,K_H,S_L,K_L}|^2 \propto e^{\frac{-S_H(S_H+1)}{2\sigma_H^2}} e^{\frac{-S_L(S_L+1)}{2\sigma_L^2}}.$$

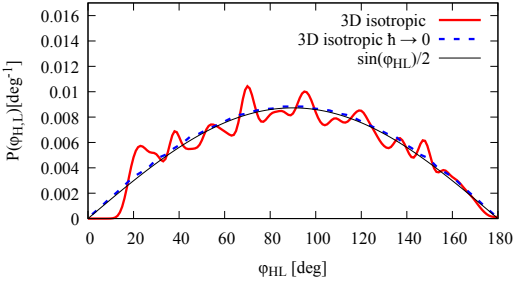

G. Scamps, PRC 109, L011602 (2024).

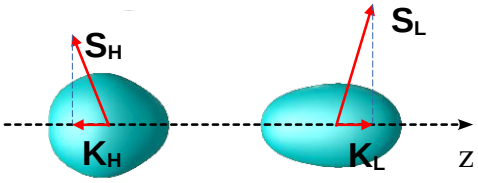

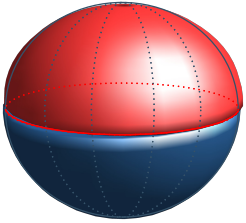

$$|\Psi\rangle = \sum_{s_H,K_H,s_L,K_L} c_{s_H,\kappa_H,s_L,\kappa_L} |S_H, K_H, S_L, K_L\rangle,$$

$$|c_{s_H,\kappa_H,s_L,\kappa_L}|^2 \propto \delta_{K_H-K_L} e^{\frac{-S_H(S_H+1)}{2\sigma_H^2}} e^{\frac{-S_L(S_L+1)}{2\sigma_L^2}}.$$

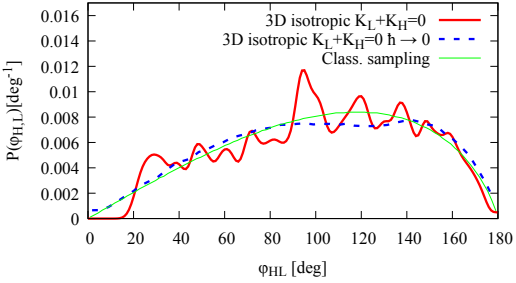

G. Scamps, PRC 109, L011602 (2024).

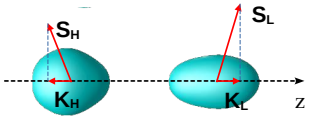

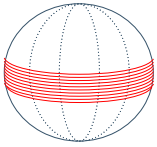

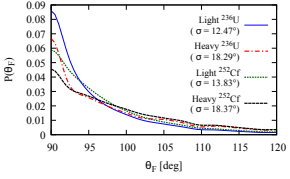

$$|\Psi\rangle = \sum_{s_H,\kappa_H,s_L,\kappa_L} c_{s_H,\kappa_H,s_L,\kappa_L} |S_H, K_H, S_L, K_L\rangle,$$

$|c_{s_H,\kappa_H,s_L,\kappa_L}|^2$ From TDDFT

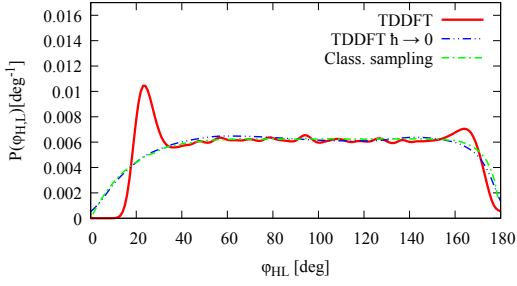

TDDFT shows an intermediate case between 2D and 3D.
G. Scamps, PRC 109, L011602 (2024).